JACS
JOURNAL OF THE AMERICAN CHEMICAL SOCIETY

Article

pubs.acs.org/JACS

Three-in-One: Sensing, Self-Assembly, and Cascade Catalysis of Cyclodextrin Modified Gold Nanoparticles

Yan Zhao,[†] Yucheng Huang,[†] Hui Zhu, Qingqing Zhu, and Yunsheng Xia*

Key Laboratory of Functional Molecular Solids, Ministry of Education; College of Chemistry and Materials Science, Anhui Normal University, Wuhu 241000, China

Supporting Information

ABSTRACT: We herein present a three-in-one nanoplatform for sensing, self-assembly, and cascade catalysis, enabled by cyclodextrin modified gold nanoparticles (CD@AuNPs). Monodisperse AuNPs 15−20 nm in diameter are fabricated in an eco-friendly way by the proposed one-step colloidal synthesis method using CD as both reducing agents and stabilizers. First, the as-prepared AuNPs are employed as not only scaffolds but energy acceptors for turn-on fluorescent sensing based on guest replacement reaction. Then, the macrocyclic supramolecule functionalized AuNPs can be controllably assembled and form well-defined one- and two-dimensional architectures using tetrakis(4-carboxyphenyl)-porphyrin as mediator. Finally, in addition to conventional host−guest interaction based properties, the CD@AuNPs possess unpredictable catalytic activity and exhibit mimicking properties of both glucose oxidase and horseradish peroxidase simultaneously. Especially, the cascade reaction (glucose is first catalytically oxidized and generates gluconic acid and H_2O_2; then the enzymatic H_2O_2 and preadded TMB (3,3′,5,5′-tetramethylbenzidine) are further catalyzed into H_2O and oxTMB, respectively) is well-achieved using the AuNPs as the sole catalyst. By employing a joint experimental−theoretical study, we reveal that the unique catalytic properties of the CD@AuNPs probably derive from the special topological structures of CD molecules and the resulting electron transfer effect from the AuNP surface to the appended CD molecules.

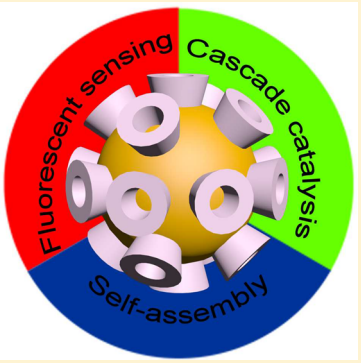

INTRODUCTION

Gold nanoparticles (AuNPs) are a continuous research interest in the fields of nanoscience and nanotechnology due to their unique optical/electrical properties and versatile application potentials.[1] Their physicochemical features and corresponding applications have aroused strong repercussions in several aspects. First, AuNPs possess a distance dependent surface plasmon resonance (SPR) band, which has been extensively employed for designing assembly/disassembly modulated colorimetric sensors.[1c,d,2] Second, the extinction coefficient of AuNPs is as high as 10^8−10^{10} M^{-1} cm^{-1}.[3] So, they are one of the ideal energy acceptors in constructing a fluorescence resonance energy transfer (FRET) system for sensing and biosensing.[1c,4] Last but not least, AuNPs exhibit catalytic activity, which makes them a potential candidate for the replacement of expensive Pt in some fields.[1b,c,5] It is widely accepted that the specific properties/applications of AuNPs are dependent on a series of factors including particle size, shape, surface chemistry, aggregation state, and preparation method.[6] For example, a relatively large size (>10 nm) is essential for distinct SPR bands;[6b] in contrast, catalytic activity is commonly believed to be the privilege of ultrasmall AuNPs (∼2 nm).[5c,e,7] In parallel, macrocyclic supramolecules, such as crown ether, cyclodextrin (CD), and calixarene, possess unique and size-tunable cavity structures and exhibit special properties.[8] On the basis of host−guest interactions, they have been well-applied for self-assembly, drug/gene delivery, separation, sensing, etc.[9] So, the integration of AuNPs and macrocyclic supramolecules not only provides a kind of hybrid nanomaterial but is expected to bring new properties, functions, and applications.[1b,10a−g]

To date, the hybrid nanomaterials consisting of macrocyclic supramolecules and AuNPs have been well-studied.[10] Despite these substantial achievements, there are a few issues and/or potential problems that are still of concern. First, in the fabrication of the hybrid entities, a few harsh reagents or conditions ($NaBH_4$, NaOH, thiols, etc.) are commonly adopted.[10e−h] In addition to being environmentally unfriendly, their extremely high binding affinity and/or strong interactions might passivate/block the surface properties of AuNPs. Second, previous studies often only focus their attention on one certain aspect of properties/applications, which is unfavorable for comprehensive understanding of the features and for better tapping of the potential of the hybrid materials. Third, in terms of the hybrid materials, pre-existing research studies mainly concentrate on their host−guest interaction based properties/functions/applications. Considering that macrocyclic supramolecules possess unique topological structures, their interactions with AuNPs might unusually modulate the particle surface chemistry and result in novel properties and corresponding potential applications.

Received: July 22, 2016
Published: December 7, 2016

DOI: 10.1021/jacs.6b07590
J. Am. Chem. Soc. 2016, 138, 16645−16654

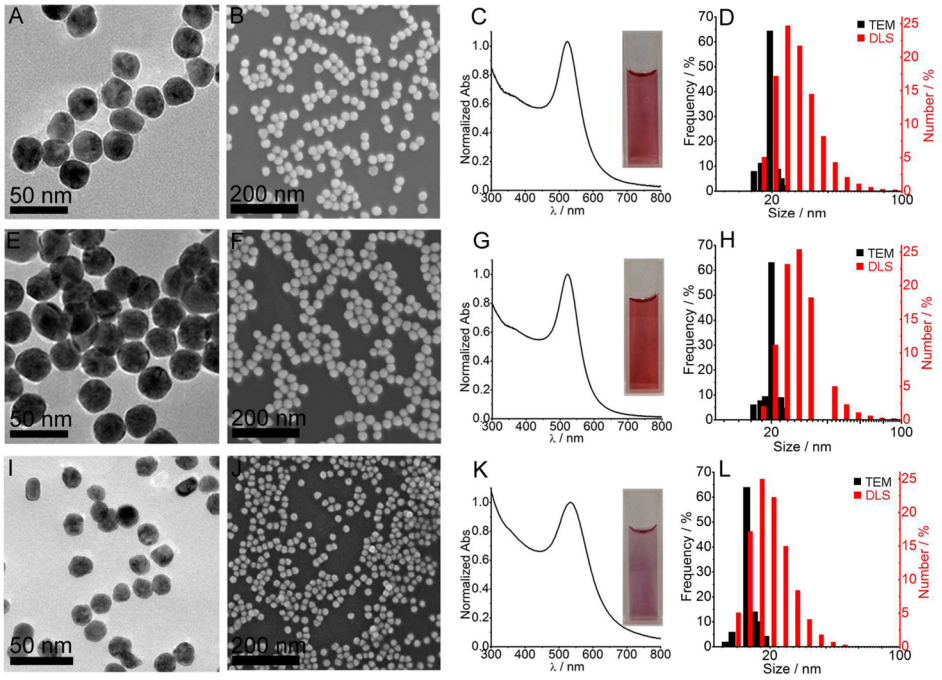

Figure 1. As-prepared CD@AuNPs. Three kinds of products made from chloroauric acid and α-CD (A–D), β-CD (E–H), and γ-CD (I–L), respectively. The four rows show TEM (A, E, I), scanning electron microscopy (SEM) (B, F, J), absorption spectra (C, G, K), and histograms of size distribution (D, H, L) results, respectively.

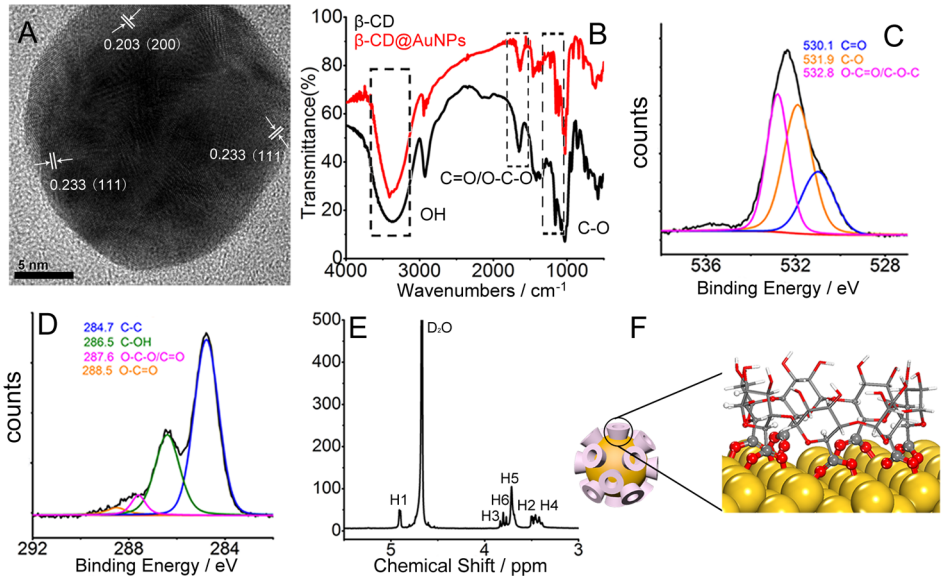

Figure 2. Structural characterizations of the β-CD@AuNPs. (A) High-resolution TEM image of the β-CD@AuNPs. (B) FT-IR spectra of the β-CD@AuNPs (red curve) and β-CD (black curve). High-resolution XPS survey scan of O 1s (C) and C 1s (D) of the β-CD@AuNPs. (E) ^{1}H NMR spectrum (in D_2O) of the β-CD@AuNPs. (F) The schematic diagram for the surface chemistry of the β-CD@AuNPs. The cartoon mode in the left of part F only shows the probable structure of the as-prepared β-CD@AuNPs, which does not consider (i) the size proportion between β-CD and the AuNPs, and (ii) the precise amounts of β-CD molecules on each AuNP.

In this study, we first demonstrate a three-in-one nanoplatform for sensing, self-assembly, and cascade catalysis enabled by CD modified AuNPs (CD@AuNPs). Monodisperse AuNPs 15–20 nm in diameter are fabricated in an eco-friendly way using CD molecules as both reducing agents and stabilizers. Different from previous approaches for the fabrication of macrocycle-AuNP hybrid nanomaterials, no harsh reagents and/or conditions are used here.[10e−g] Because the AuNPs possess supramolecular cavities on their surface, they can be employed as scaffolds and energy acceptors for turn-on fluorescent sensing by host–guest interactions. Then, the CD@AuNPs can act as building blocks and assemble into well-defined one- and two-dimensional (1D/2D) superstructures with the assistance of tetrakis(4-carboxyphenyl)porphyrin (TCPP) as mediator. Finally, despite being tens of nanometers in diameter, the AuNPs possess unpredictable catalytic activity and exhibit mimicking properties of both glucose oxidase (GOx) and horseradish peroxidase (HRP) simultaneously.

DOI: 10.1021/jacs.6b07590
J. Am. Chem. Soc. 2016, 138, 16645–16654

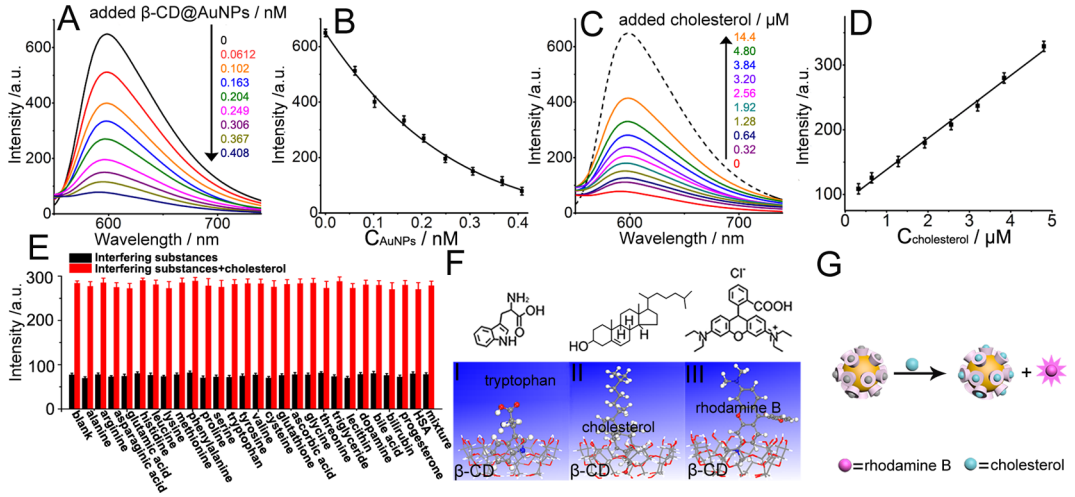

Figure 3. Fluorescent sensing of cholesterol using the composite made of the β-CD@AuNP and RB molecules. (A) Fluorescence spectra of RB in the presence of different concentrations of the AuNPs. (B) Plots of RB fluorescence intensities versus the AuNP concentrations. (C) Fluorescence spectra of the (β-CD@AuNP-RB) composite after adding varying amounts of cholesterol. (D) Plots of the (β-CD@AuNP-RB) composite fluorescence intensities versus cholesterol concentrations. (E) Selectivity of the (β-CD@AuNP-RB) composite toward various potential interfering substances. The concentration of cholesterol is 4.0 μM; the concentrations of the added various substances (from alanine to lecithin) are 0.3, 0.1, 0.08, 0.12, 0.12, 0.16, 0.2, 0.02, 0.08, 0.26, 0.14, 0.06, 0.08, 0.16, 0.25, 1.0, 0.1, 0.28, 0.16 1.04, 2.5 μM, respectively; the concentrations of dopamine, bile acid, bilirubin, progesterone, and HSA (human serum albumin) are 3.0 pM, 4.9 nM, 9.4 nM, 4.5 pg/mL, and 0.035 g/L, respectively. The concentrations of both the analytes and various potential interfering substances correspond to 1000 times dilution of those in serum. (F) DFT models for the interactions of β-CD with tryptophan (I), cholesterol (II), and RB (III), respectively. Also, the chemical structures of the three kinds of guest molecules are displayed. (G) Schematic illustration of fluorescent turn-on detection of cholesterol using the (β-CD@AuNP-RB) composite.

Especially, the cascade reaction (glucose is first catalytically oxidized and form gluconic acid and H_2O_2; then the enzymatic H_2O_2 and preadded 3,3′,5,5′-tetramethylbenzidine (TMB) are further catalyzed into H_2O and oxTMB, respectively) is well-achieved using the AuNPs as the sole catalyst. By combination of experiments and density functional theory (DFT) calculations, the unpredictable catalytic properties of the CD@AuNPs probably derive from the unique topological structures of CD molecules and the resulting electron transfer effect from the AuNP surface to the appended CD molecules.

RESULTS AND DISCUSSION

We found that AuNPs could be facially fabricated using CD molecules as both stabilizers and reducing agents in mild conditions. After the mixture of CD molecules, chloroauric acid, and phosphate buffer solution (PBS, pH 7.0) was heated to 100 °C for 60 min (Figures S1−S4 in Supporting Information), Au colloidal solution was reliably obtained (Figure S5 in Supporting Information). Figure 1 shows three kinds of AuNPs synthesized by the CD molecules with different sized cavities, namely, α-, β-, and γ-CD, respectively. The three corresponding AuNPs are 19 ± 1.8, 20 ± 1.6, and 15 ± 1.8 nm in diameter, as determined by transmission electron microscopy (TEM). According to dynamic light scattering (DLS), their average hydrodynamic diameters are 22, 24, and 19 nm, respectively, in agreement with TEM measurements, despite some apparent enlargement because of a hydration layer and a stronger contribution of larger particles to DLS signal.[11] For the β-CD@AuNPs, their shape is spherical/quasispherical with only 8% size distribution (Figure 1E,F). The AuNP solution is wine red and possesses a sharp SPR band centered at 520 nm (Figure 1G), indicating the typical features of gold nanosphere. While for the α- and γ-CD@AuNPs (Figure 1A,I), slightly elongated NPs are occasionally observed. Accordingly, the solutions are somewhat purple, and the SPR bands exhibit a little broadening with small trailing over 750 nm (Figure 1C,K). Because β-CD had the best performances in the AuNP fabrication, the corresponding products were then employed for further study.

As shown in Figure 2A, the β-CD@AuNPs are 5-fold twin crystalline, similar to the products obtained by the conventional Turkevich method.[12] The AuNPs possess distinct lattice fringes, indicating good crystallinity. We then employed various characterization techniques to detect the surface chemistry of the products. The Fourier transform infrared spectroscopy (FT-IR) spectra of β-CD and the β-CD@AuNPs were first detected. As shown in Figure 2B, the similar profiles of the two curves preliminarily indicate that the major feature groups of β-CD molecules are retained in the obtained products. Furthermore, the hydroxy band (3354.7 cm^{-1}) of the products is obviously narrower than that of the original β-CD, demonstrating the decrease in the amounts of hydroxy groups.[13] Because O—C—O and C═O groups have a similar stretching vibration,[14] X-ray photoelectron spectroscopy (XPS) was then used to further detect the structure information. The O 1s XPS spectrum (Figure 2C) exhibits three peaks at 531.9, 530.1, and 532.8 eV, which are attributed to C—O, C═O, and O—C═O/C—O—C, respectively,[15] while for the C 1s spectrum (Figure 2D) four peaks at 284.7, 286.5, 287.6, and 288.5 eV are observed, resulting from C—C, C—OH, O—C—O/C═O, and O—C═O bonds, respectively.[14−16] According to the contrast of XPS data (Figure 2D versus Figure S6B in Supporting Information), a new group, namely, a carboxyl, is produced in the as-prepared β-CD@AuNPs. On the basis of the decrease of hydroxy and the appearance of carboxyl groups, the chemical processes on the formation of the AuNPs can be simply understood as hydroxy groups in CD reduce Au^{3+} into Au^0, which leads to nucleation, growth, and formation of Au particles; at the same time, the hydroxy groups themselves are oxidized to carboxyl ones (Scheme S1 in

DOI: 10.1021/jacs.6b07590
J. Am. Chem. Soc. 2016, 138, 16645−16654

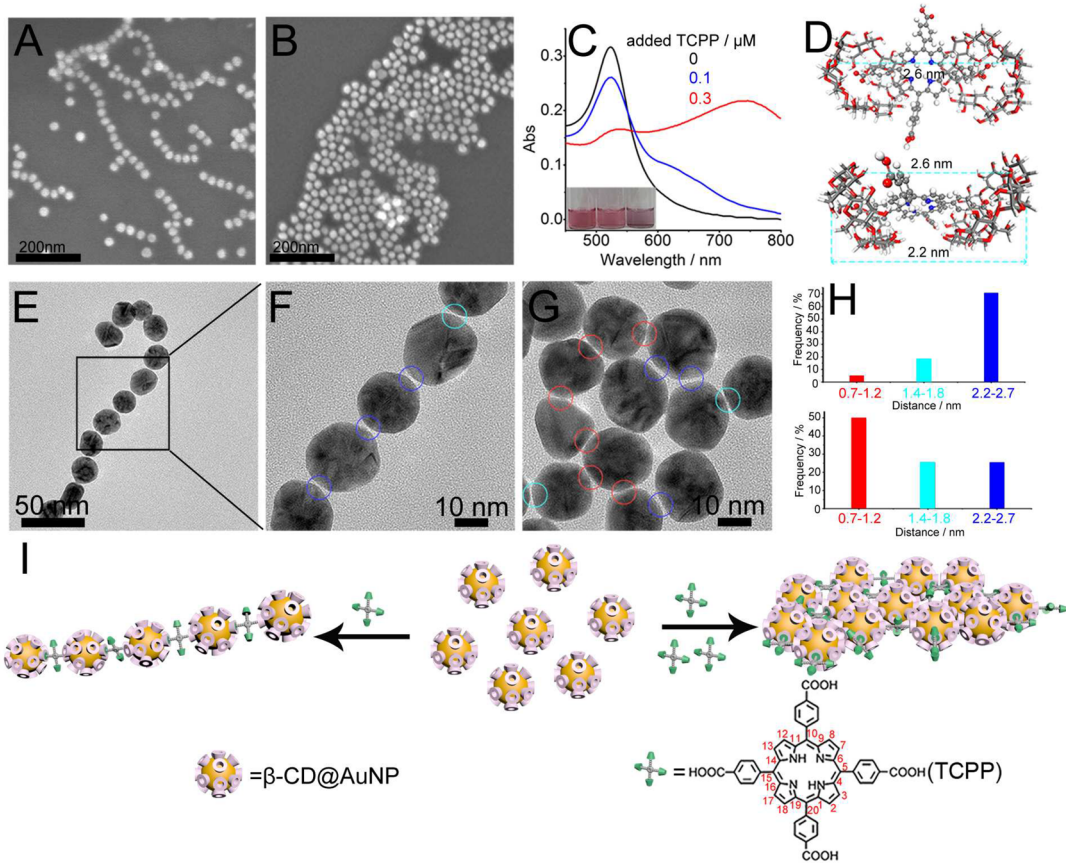

Figure 4. 1D and 2D self-assembly of the β-CD@AuNPs. SEM images of the 1D (A) and 2D (B) assemblies of the β-CD@AuNPs in the presence of 0.1 and 0.3 μM TCPP molecules, respectively. (C) The absorption spectra and photo images (inset) of the β-CD@AuNPs in the presence of different concentrations of TCPP molecules, which correspond to parts A and B. (D) Sketch of two β-CD rings connected by a TCPP molecule by para (5,15) host–guest interactions (above, top view; below, side view). TEM images of 1D (E, F) and 2D (G) assemblies of the β-CD@AuNPs in the presence of 0.1 and 0.3 μM TCPP molecules, respectively. The different particle–particle distances are highlighted by different colored circles, which are correspond to part H. (H) Histograms for the distances among particle–particle interactions in the 1D assembly (above) and the 2D assembly (below). The two histograms are the results of 150 particle–particle distances, respectively. In the statistics, only the particle–particle distances within 0.5–3.0 nm are counted. (I) Schematic illustration of the 1D/2D self-assembly of the AuNPs based on TCPP concentration modulated by host–guest interactions.

Supporting Information). Furthermore, the formed carboxyl groups interact with the Au particle surface by O—Au conjunction[10g] and prevent unlimited growth and/or agglomeration of the AuNPs. As shown in Figure 2E, six different chemical shifts of the β-CD@AuNPs are detected by ^{1}H NMR spectra (300 MHz, in D_2O), which corresponds well with β-CD molecules themselves, as shown in Figure S7 and Table S1 (Supporting Information). This result indicates that the macrocycle structure of β-CD is well-maintained after the reaction.[17]

Because ligand density has profound effects on NP properties,[18] we employed the combination of ^{1}H NMR[19] and UV–vis absorption[3] spectroscopy to estimate this value. On the basis of Figure S8 (Supporting Information), there are about 73 β-CD molecules on each AuNP surface. The ξ-potential values of the AuNP containing solutions are −19.5 to −38.2 mV depending on pH values (Figure S9 in Supporting Information). Such negative surface charges can help to stabilize the AuNPs by electrostatic repulsion. As shown in Figure S10 in Supporting Information, the AuNPs can remain very stable in the presence of 10 mM NaCl salt. Due to higher activity, we propose that primary hydroxy groups (namely, at the smaller side of β-CD) are preferentially oxidized and form carboxyl groups, which then bind onto the AuNP surface.[20] According to the above, the schematic diagram for the surface chemistry of the CD@AuNPs is sketched in Figure 2F.

The supramolecular macrocycles on the AuNP surface can act as scaffolds for organic fluorophores, and the formed composites are promising for the employment of FRET based chemosensors.[21] To demonstrate the potential applications, the interactions of the AuNPs and rhodamine B (RB) molecules were first studied. As shown in Figure 3A,B, the fluorescence of RB is gradually quenched with an increase of the added AuNPs. Because of matchable size/structure, the fluorophores can enter into the macrocyclic cavity by host–guest interactions. As a result, an effective energy transfer from the fluorophores to the AuNPs occurs, which results in fluorescence quenching. The quench efficiency can reach 90.2% in the presence of 0.408 nM AuNPs.

As cholesterol molecules were introduced into the (β-CD@AuNP-RB) composite system, the quenched fluorescence is gradually restored, as shown in Figure 3C. There is a good linear relationship (R = 0.994) between the fluorescence intensities and the concentrations of cholesterol in the range 0.32–4.80 μM (Figure 3D), and the detection limit is as low as 0.15 μM (signal-to-noise ratio of 3). Such fluorescence recovery

DOI: 10.1021/jacs.6b07590
J. Am. Chem. Soc. 2016, 138, 16645–16654

results from the replacement between cholesterol and RB molecules.[21] Then, to further demonstrate the work principle, the fluorescence responses of the (β-CD@AuNP-RB) composite toward two other cholesterol analogues, namely, bile acid and β-sitosterol, were then studied. As shown in Figure S11 in Supporting Information, β-sitosterol exhibits a similar fluorescence recovery behavior; in contrast, bile acid only leads to a very limited fluorescence recovery. In a comparison with cholesterol and β-sitosterol, bile acid is more hydrophilic, which is adverse to their interaction with the hydrophobic supramolecular cavity. These results, on one hand, further verify the replacement mechanism shown in Figure 3G; on the other hand, they indicate that the present platform is promising for the sensing of hydrophobic sterols.

Furthermore, in light of the importance of the blood cholesterol assay, the relevant selectivity was accordingly investigated. In terms of the selectivity, three points should be noted (Figure 3E). First, the commonly coexisting biomolecules, including various amino acids, ascorbic acid, dopamine, human serum albumin, glutathione, bilirubin, triglyceride, lecithin, and progesterone, have little effect on the fluorescence intensities of the (β-CD@AuNP-RB) composite system; furthermore, they almost do not interfere with the analyte induced fluorescence recovery. Second, in addition to a weaker fluorescence response, the concentration of blood bile acid is about 3 orders of magnitude lower than that of cholesterol,[22] so it does not impact cholesterol assay. Third, tryptophan does not interfere with the assay, although tryptophan and CD can also form an inclusion complex by host−guest interactions.[23] To understand such exclusive responses to the analytes, DFT calculations were performed (Figure 3F). The interaction energies (the definition can be seen in the Calculations section in the Supporting Information) of the three kinds of the host−guest complexes, namely, CD-tryptophan, CD-cholesterol, and CD-RB, are −0.84, −1.37, and −1.01 eV, respectively. Herein, a more negative energy value means better stability of the resulting complexes. Because of the lower stability, tryptophan cannot effectively replace RB from the CD cavity; in contrast, the interaction energy of CD-cholesterol is somewhat more negative than that of CD-RB, which promotes well the guest replacement reaction.

Finally, to assess the applications of the present system, the assay of cholesterol in human serum was studied. As shown in Table S2 in the Supporting Information, for all samples, whether from male or female, the measured concentrations of endogenous cholesterol are in agreement with the results obtained by the commercial monitor on the whole. Then, recovery tests of the standard addition method show that their recovery rates range from 94.0% to 109.0%. These results indicate the application potential of the proposed sensing platform.

AuNP based self-assembly has attracted considerable attention because it is an ideal platform for studying the fundamental science of NP interactions at nanoscale; furthermore, it is a facile and effective system for various assay/bioassay applications. We envisioned that the as-prepared macrocycle functionalized AuNPs were promising as building blocks for self-assembly by host−guest interactions.[10a,d,e,g,24] Toward this goal, TCPP (its structure is shown in Figure 4) was chosen as mediator for two reasons. First, it can react with β-CD by host−guest interactions (Figure S13 in Supporting Information); then, each TCPP molecule has four donors, which provide multiple possibilities for the host−guest interactions and might facilitate modulation of the CD@AuNP assembly behaviors. As 0.1 μM of TCPP was introduced into the AuNPs containing solution, distinct 1D chain-like self-assembled architectures were obtained (Figure 4A). Interestingly, the AuNPs could further assemble into 2D network-like superstructures as the mediator concentration was enhanced to 0.3 μM (Figure 4B). In addition to the hydrophilic SiO_2 substrate, similar 1D and 2D assemblies were also observed at the hydrophobic carbon film, as shown in TEM images (Figure 4E−G, and Figures S14 and S15 in Supporting Information). Herein, the used substrates had little effect on the structures of the products, demonstrating that (i) the assembly processes occurred in bulk solution instead of dry on substrate; and (ii) the obtained architectures were rather robust. The assembly processes were so distinct that they could be observed even by naked eyes. As shown in the inset of Figure 4C, the AuNP solution changes from wine red to somewhat purple in the presence of 0.1 μM TCPP, which further become purple with 0.3 μM TCPP. Meanwhile, the SPR peak at 520 nm shows a gradual intensity decrease, and a new SPR band at 600−800 nm appears simultaneously. Absorption spectroscopy is an in situ detection technique, so the observed changes in the absorption profiles and solution color further demonstrated that the self-assembly of the AuNPs happened in solution.

To date, AuNP assemblies with 1D/2D/3D topological structures have been extensively studied and reported.[25] However, good modulation of the assembly dimensionality without any templates/scaffolds (carbon nanotubes, DNA, two phase interface, etc.) has been a challenging issue, especially for well-defined 1D and 2D superstructures.[25a,26] Unlike semiconductor quantum dots,[27] metallic NPs exhibit no intrinsic electric dipole. So, the fundamental science for the formation of anisotropic 1D/2D metal NP assemblies has remained an open question, although a few phenomenological explanations have been proposed for respective systems. In the present system, the formation of the AuNP assemblies might be ascribed to the balance of several effects, namely, host−guest interaction, steric effect, van der Waals attraction, electrostatic repulsion, etc.

The added TCPP molecules have two effects on the AuNP assembly system. On one hand, they lead to unique and dimension related particle−particle distances in the resulting self-assemblies. As shown in Figures S16 and S17 in Supporting Information, in terms of two other kinds of samples, namely, direct dry on TEM grid and NaCl induced aggregation/assembly, the adjacent AuNPs are very close and even directly contact each other. As described previously, there are about 73 β-CD molecules on each AuNP. The distance between the two adjacent attached β-CD molecules is about 4.7 nm assuming that the β-CD molecules are evenly distributed on the AuNP surface. Such relatively low stabilizer coverage allows the AuNPs to be in close contact during their drying on a TEM grid. However, this situation is changed in the presence of TCPP molecules, and both 1D and 2D products exhibit well-defined particle−particle distances. As shown in Figure 4F and Figure S14 (Supporting Information), for 1D self-assembly, ∼2.5 nm (2.2−2.7 nm) intervals among the AuNPs are considerably dominant (more than 50%). While for 2D assemblies, the situation is relatively complex (Figure 4G and Figure S15 in Supporting Information): A few particles are about 2.5 nm apart, which is similar to that of the 1D one, while more AuNPs are closer (∼1 nm) to each other. Basically, the particle intervals directly demonstrate the host−guest interaction modulated self-assembly: The formation of CD-TCPP-

DOI: 10.1021/jacs.6b07590
J. Am. Chem. Soc. 2016, 138, 16645−16654

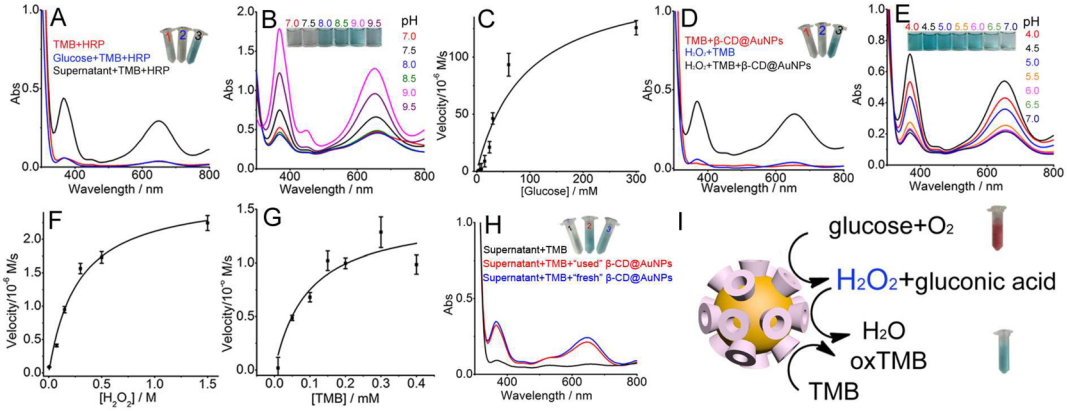

Figure 5. Catalytic properties of the β-CD@AuNPs. (A) Absorption spectra of three TMB related systems. The supernatant came from the CD@AuNPs-glucose system. After catalysis, the AuNPs were separated by centrifugation, and the resulting supernatant was obtained. (B) pH dependent GOx-mimicking property of the AuNPs. (C) Steady-state kinetic assay of GOx-mimicking activity. The velocity (ν) of the reaction was measured using 0.605 nM AuNPs. (D) Absorption spectra of three TMB based systems. (E) pH dependent HRP-mimicking property of the AuNPs. (F, G) Steady-state kinetic assay of HRP-mimicking activity. The velocity (ν) of the reaction was measured as the concentration of the AuNPs was 0.09 nM. In part F, the concentration of TMB was 0.12 mM. In part G, the concentration of H_2O_2 was 6 mM. (H) TMB chromogenic reaction systems for H_2O_2 produced by the catalysis of glucose using β-CD@AuNPs as the catalyst. The pH values of all supernatants had been tuned to 4.5. The "used" AuNPs meant the AuNPs had been used for the first-step GOx-mimicking catalysis. The "fresh" AuNPs meant the AuNPs had not been employed for the catalysis of glucose oxidation. (I) Schematic illustration of the cascade catalysis system using the β-CD@AuNPs as the only catalyst.

CD superstructures between the AuNPs can effectively prevent the direct contact of the building blocks. Then, the different particle−particle distances of 1D and 2D architectures can give some information on the assembly processes (see below). On the other hand, as one kind of electrolyte, TCPP molecules can enhance the ionic strength and screen the repulsive electrostatic forces among the dispersed AuNPs. The ξ-potential values of the AuNP solution change from −19.5 to −7.43 and −4.62 mV in the presence of 0.1 and 0.3 μM TCPP molecules, respectively (Figure S18 in Supporting Information).

Let us then consider several dimension relevant parameters, which are helpful for understanding the self-assembly behaviors. First, the size of the AuNPs is 20 nm. Second, at the AuNPs' surface, the distance of the two adjacent β-CD molecules is about 4.7 nm (see previously). Third, TCPP molecules are approximately 2 nm in diameter, and their two benzoic acid groups at ortho (5,10) positions are 1.2 nm apart. The four dimensions are defined as d_{AuNPs}, $d_{CD\text{-}CD}$, d_{TCPP}, and $d_{5,10}$, respectively. Accordingly, for the TCPP molecule, its four donors are impossible to simultaneously interact with the CD molecules on the AuNPs' surface due to space and steric hindrance ($d_{TCPP} \ll d_{AuNPs}$); furthermore, its two donors at ortho (5,10) positions cannot interact with the acceptors located at the same AuNP ($d_{5,10} < d_{CD\text{-}CD}$). As a result, in terms of the interactions of TCPP and the appended CD molecules, the formation of the host−guest complexes with 1:3 and 1:4 ratios can be excluded. Of course, only 1:2 complexes (include both para (5,15) and ortho (5,10) position based interactions) have a direct contribution on the host−guest interaction modulated self-assembly. In terms of the particle intervals, ∼2.5 nm just corresponds to the lengths of the sandwich structure consisting of two CDs and one TCPP based on para (5,15) host−guest interactions, while for ortho (5,10) interactions, the minimum and the maximum of the particle distances are ∼1 and ∼1.5 nm, respectively (Figure S19B1,B2 in Supporting Information).

On the basis of the above analysis, the present controllable 1D/2D self-assembly can be qualitatively explained as follows. In the presence of lower concentration (0.1 μM) of TCPP molecules, despite some screening effect, the remaining electrostatic repulsive effects are still rather strong. So, in terms of the TCPP modulated self-assembly, on the one hand, to minimize the electrostatic repulsion between the two building blocks, the host−guest bridging would preferentially adopt the para position (5,15) mode, as demonstrated by the characteristic 2.5 nm particle interval (top of Figure 4H). On the other hand, for minimizing the system energy, the AuNPs tend to choose 1D self-assembly. Geometrically, for 1D architectures, there are minimal (only two) particles around each building block as compared with their 2D and 3D counterparts. In this regard, 1D chains probably possess the lowest system energy because of the smallest repulsion among the particles. As the mediator concentration is further increased (0.3 μM), distinct 2D products are obtained (Figure 4B,G). In higher concentrations of TCPP, the further decreased electrostatic repulsion is in favor of higher dimensional assembly; then, the law of mass action pushes ortho (5,10) position based interactions to also occur simultaneously (the right of Figure 4I), as indicated by the smaller particle−particle distance (on the basis of statistical results shown in Figure 4H, in 2D self-assembly, ∼1 nm distance is dominant, which just corresponds to the shortest interval of ortho (5,10) based interactions). Both of the two effects cause the resulting 2D architecture. In both 1D and 2D self-assemblies, the ∼1.5 nm distance among the AuNPs is observed. Such an interval is probably produced by ortho (5,10) based self-assembly, and the para (5,15) based one is also possible, considering the projection effect in TEM imaging. Because of different intervals among the building blocks, the 2D products are somewhat random in appearance instead of a regular lattice.[28] In the experiments, except for a few very limited and local layer stacking structures (red circles in Figure S20 in Supporting Information), well-organized 3D architectures are not observed with even a further increase of the mediator concentration. This result indicates that the stereohindrance effect, resulting from the bulky appended CD molecules, probably also plays an important role in the assembly. So, in brief, the competition of the two opposite effects, namely, host−guest bridging and electrostatic/steric

DOI: 10.1021/jacs.6b07590
J. Am. Chem. Soc. 2016, 138, 16645−16654

repulsion, leads to the unique dimension modulated architectures. Interestingly, in the TCPP induced AuNP assembly system, the introduction of cholesterol molecules could cause a gradual recovery of the AuNP absorption spectra (Figure S22 in Supporting Information), indicating that this assembly is partially reversible. As far as we know, it is the first report that dimension controllable nanoassembly is achieved by host−guest interaction modulation, using CD@AuNPs as building blocks. Furthermore, on the basis of rationally designing the structure of guest molecules, it is possible to regulate the AuNP intervals, which is significant in the study of plamson coupling, surface enhanced Raman scattering, etc.

Due to comparable size, shape, charge, and surface chemistry, inorganic NPs possess a few properties and functionalities (such as self-assembling into complex microscale superstructures, enzymatic activity, etc.) similar to those of nature proteins.[29] Especially, several groups have reported that dispersed AuNPs without any supports can catalyze glucose into gluconic acid and H_2O_2.[5c,d,30] Inspired by these studies, we first evaluated the GOx-mimicking activity of the as-prepared AuNPs. The AuNPs were incubated with glucose at room temperature for 30 min, and the resulting solution was interrogated with a gluconic-acid-specific colorimetric assay. When hydroxylamine and Fe^{3+} were added to the solution,[31] the color of the solution turned to orange, and a distinct absorbance band at 500−700 nm appears (Figure S23 in Supporting Information), indicating that gluconic acid was indeed produced in the AuNP-glucose system. Furthermore, another enzymatic product, H_2O_2, was also verified, as demonstrated by its characteristic chromogenic agent (TMB as the substrate, inset of Figure 5A). Similar to GOx, the catalytic activity of the AuNPs is also strongly dependent on the medium's pH. According to Figure 5B, pH 9 is the best condition for the catalysis. The kinetic data were obtained by varying one substrate concentration while keeping the other substrate concentration constant. A series of initial reaction rates are calculated and applied to $\nu = V_{max}[S]/(K_m + [S])$,[32] where ν is the initial velocity, [S] is the concentration of the substrate, K_m is the Michaelis−Menten constant, and V_{max} is the maximal reaction velocity. As shown in Figure 5C, the catalysis process can be well-described by the typical Michaelis−Menten curve, and the fitted parameters are displayed in Table S3 (Supporting Information). The K_m value is 92.19 ± 5.43 mM, which is higher than that of GOx.

Surprisingly, we found that the CD@AuNPs also possessed HRP-mimicking activity (Figure 5D). As shown in Figure 5E, the AuNPs exhibit the best catalytic performances at weaker acid medium (pH 4.5). The above method was used in the determination of the HRP-mimicking catalytic property. In Figure 5F, the K_m value of the AuNPs (Table S4 in Supporting Information), using H_2O_2 as the substrate, is 272.78 ± 32.06 mM. This value suggests that the AuNPs have a lower affinity for H_2O_2 than that of HRP. Also, as described in Figure 5G, the K_m value of the AuNPs is 0.094 ± 0.0075 mM (Table S4 in Supporting Information) as TMB is employed as the substrate. This value is obviously smaller than that of HRP, indicating that the AuNPs have a higher affinity toward TMB (see below).

Because the AuNPs could act as both GOx- and HRP-mimicking for the corresponding catalytic reactions, we then studied whether the cascade reaction, namely, from glucose to gluconic acid and H_2O_2, then further to H_2O and oxTMB (TMB was preadded), could be performed by the sole CD@AuNPs. The AuNPs were first incubated with glucose at pH 9.0 PBS for 30 min. Then, the solution was centrifuged to separate the AuNPs. After the supernatant was tuned to pH 4.5 by acetate buffer solution, the centrifugally separated AuNPs (redispersed in 200 μL of water) were added again (herein, the separation of the AuNPs after the first step of the reaction was to avoid their aggregation during the pH adjustment from 9.0 to 4.5 by acetate buffer solution). Indeed, the cascade catalysis reaction was achieved as demonstrated by the blue color of oxTMB, as shown in the inset of Figure 5H. Furthermore, the HRP-mimicking performance of the AuNPs was almost invariable after the first-step glucose catalysis, as compared with that of the "fresh" CD@AuNPs (the only employment for the second-step HRP-mimicking catalysis, Figure 5H). The results indicated that the CD@AuNPs were rather robust and competent for the cascade reaction (Figure 5I). Previously, the study of the catalytic properties of AuNPs were only focused on the one-step reaction, and the cascade reaction was often realized by composite/hybrid materials made of two kinds of catalysts.[33] To our knowledge, this is the first report that the cascade reaction is achieved by using AuNPs as the sole catalyst.

It is interesting to ask why the as-prepared AuNPs have this unexpected catalytic activity, especially when the diameter of the particle is as large as 20 nm. As shown in Figures 1 and 2A, the CD@AuNPs are spherical/quasispherical. So, the AuNPs have mixed facets containing both low- and high-index faces instead of the single one. As a result, we first envisioned whether the catalytic activity came from the high-index facets, based on the reports of previous literature studies.[34] To verify this point, two other kinds of AuNPs were fabricated on the basis of the same method; only CD molecules were replaced by glucose and citrate, respectively. The two products are also spherical, and their sizes are 50 and 13 nm (Figure S24A,B in Supporting Information). As shown in Figure S24C,D (Supporting Information), both of them were almost HRP-mimicking inert. We then studied the effects of CD molecules, considering that CD based composites had been employed as peroxidase mimicking.[35] As described in Figure S25 (Supporting Information), CD itself had almost no any peroxidase activity. Finally, we checked the α-CD@AuNPs and found that they also had the HRP-mimicking property; however, the activity was somewhat lower than that of β-CD@AuNPs (Figure S26 in Supporting Information). On the basis of the above three sets of control experiments, the present unique catalytic properties of the CD@AuNPs should result from the synergistic effects of CD molecules and Au particles.

To understand the catalytic property of the as-prepared CD@AuNPs, DFT calculations were performed to study the electronic states of the AuNP surface. Here we chose three low-index gold facets, named (111), (100), and (110), for the calculations. The binding energies of carboxylated β-CD on the Au(111), Au(100), and Au(110) surfaces were calculated to be 10.8, 12.4, and 15.9 eV, respectively (Figure 6A−C). The high binding energy stems from the strong binding of O atoms to the surface, where O atoms act as anchors. The binding strength order is in excellent agreement with the sequence of coordination number (CN) of Au on the three surfaces; that is, from Au (111) to (100) to (110), the CN decreases from 9 to 8 to 7, and the binding energy increases monotonously and linearly. It is interesting that, according to Bader charge analysis,[36] Au atoms which are in contact with the anchored O are electropositive (+0.2 to +0.3 e) (Figure 6D), but the remaining ones are still electroneutral.

DOI: 10.1021/jacs.6b07590
J. Am. Chem. Soc. 2016, 138, 16645−16654

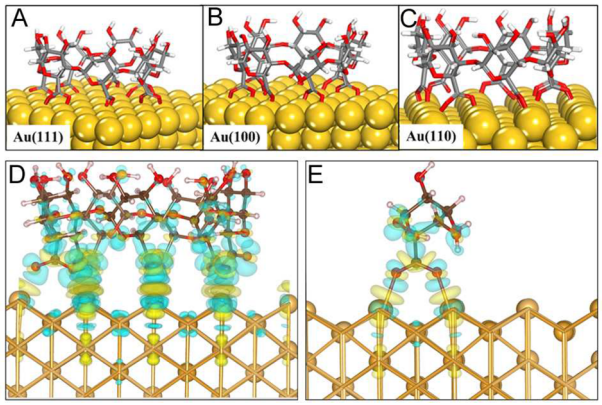

Figure 6. Carboxylated β-CD molecules adsorb on Au(111) (A), Au(100) (B), and Au(110) (C) surfaces. Charge density differences of the carboxylated β-CD (D) and carboxylated glucose (E) adsorbed on the Au (110) surface. The light green and light yellow regions represent charge depletion and accumulation, respectively.

Previously, Rossi and co-workers studied glucose oxidation catalyzed by AuNPs,[37] and they proposed a plausible mechanism: Glucose first forms a hydrated glucose anion, which then interacts with the gold surface to stimulate molecular oxygen and forms gold containing intermediates, and finally, the reaction products are produced by electron transfer processes from the two α-H at the C atoms linked with the $Au^{+}-O$ to the O−O group. Such a mechanism is probably suitable for the present system. However, there were a few differences as the CD@AuNPs were used as the catalyst. Because of electron transfer effects from the AuNPs to CD molecules, the AuNPs possessed a unique positively charged surface. In comparison with previous AuNPs with a neutral surface, such a positively charged one should possess a higher affinity toward the hydrated glucose anion, which greatly facilitated formation of the intermediates and the catalytic reactions. According to the above, the proposed reaction processes using the CD@AuNPs as the catalyst are shown in Scheme S2 in Supporting Information.

In terms of the HRP-mimicking property, we suppose that $HO^{\bullet}$ radicals might participate in the reaction system, considering that H_2O_2 molecules and $HO^{\bullet}$ radicals have a close connection. To demonstrate this point, a fluorescence technique was employed to detect the status of $HO^{\bullet}$ formation in solution using terephthalic acid molecules as probes.[38] As shown in Figure S28 (Supporting Information), the more CD@AuNPs that were added, the stronger the fluorescence intensities that were observed. These results indicated that the $HO^{\bullet}$ radicals were produced indeed in the presence of the CD@AuNPs.[38] So, the HRP-mimicking properties could be preliminarily understood as $HO^{\bullet}$ radicals were formed from H_2O_2,[5c] which then oxidized the preadded TMB and produced blue oxTMB.[39] At present, the exact effects of the positively charged surface on the generation of $HO^{\bullet}$ radicals are unknown. However, it is plausible that such positively charges sites are helpful for the $HO^{\bullet}$ radical related catalytic reactions because of the following reasons: Generally, the lifetime of radicals is transient, which is against the corresponding catalytic reaction. The positively charged gold interface probably stabilized the generated $HO^{\bullet}$ radicals via an electron exchange interaction,[40] which effectively extended the lifetime of $HO^{\bullet}$ radicals and enhanced the catalytic reactivity. Furthermore, the used substrate, namely, TMB, can interact with CD molecules by host−guest interactions (Figure S29 in Supporting Information). As a result, the affinity of the AuNPs and TMB (K_m: 0.094 mM) is even higher than that of HRP (K_m: 0.434 mM).

To further understand the effects of CD molecules on the catalytic properties, we then calculated the interactions of a carboxylic glucose molecule, namely, the monomer of CD, with the Au surface. Its binding energies on the Au(111), Au(100), and Au(110) are 1.66, 1.82, and 2.30 eV, respectively. Upon multiplication of 7 by these numerical values, the results are very close to those of β-CD on the surfaces, since each β-CD contains 7 glucose monomers. On the basis of these data, the resulting positively charged Au surface and corresponding catalytic properties of CD@AuNPs probably result from the unique structure of CD molecules: In each CD, several (6−8) glucose molecules connect each other and form a fixed ring shaped structure. As they interact with the Au surface, their multiple binding sites are confined in a very limited space by the ring structure. The electron transfer effect at these positions is accordingly dramatic, which then act as active sites for the catalytic reactions. In contrast, for glucose molecules, on one hand, the binding energy is smaller, and the electron transfer effect is weaker (Figure 6E). On the other hand, they probably evenly adsorb on the Au surface although a few facets might have priority. However, generally, the adsorption should be random and cannot form enough positively charged points on a Au surface. As a result, their catalytic activity is correspondingly weak.

According to the above study, the catalytic properties of the products result from the synergistic effects of the two components; namely, the appended CD molecules delicately modulate the electronic states of the AuNPs due to their special topological structures. As shown in Figure S30 in Supporting Information, the β-CD@AuNPs exhibit almost no HRP-mimicking activity as the AuNPs interact with mercaptoethanol. Because of a stronger affinity between S and Au atoms, the thiols could bind onto the AuNP surface, and further exchange of the appended CD molecules was also possible. As a result, the AuNPs were passivated, and the catalytic activity was correspondingly blocked. So, the surface chemistry of AuNPs is very critical to their catalytic properties, and the β-CD@AuNPs are not an exception.

■ CONCLUSION

In summary, we present an eco-friendly method for one-step fabrication of supramolecule functionalized AuNPs using CD molecules as both stabilizers and reducing agents. Because the AuNPs possess macrocyclic structures on the particle surface, they can be employed as scaffold and energy acceptor for fluorescent sensing. Furthermore, the CD@AuNPs act as building blocks for the construction of well-defined nanosuperstructures: 1D/2D architectures are well-obtained by simple modulation of mediator (TCPP) concentrations. In addition to conventional host−guest interaction based properties, the CD@AuNPs can achieve unique cascade catalysis. Such properties probably result from the specific topological structures of CD molecules and their unique electron transfer effects with the appended Au surface. This contribution, on one hand, demonstrates that the familiar AuNPs still have some "hidden" features; on the other hand, ligand structure design might be an alternative strategy for manipulating the physicochemical properties of metal NPs beyond particle size and crystal face, especially for catalysis.

DOI: 10.1021/jacs.6b07590
J. Am. Chem. Soc. 2016, 138, 16645−16654

■ ASSOCIATED CONTENT

Supporting Information

The Supporting Information is available free of charge on the ACS Publications website at DOI: 10.1021/jacs.6b07590.

Experimental and theoretical calculation details, reagents and instruments used, and supplementary figures and tables (PDF)

■ AUTHOR INFORMATION

Corresponding Author

*xiayuns@mail.ahnu.edu.cn

ORCID

Yunsheng Xia: 0000-0002-7877-9718

Author Contributions

†Y. Zhao and Y. Huang contributed equally.

Notes

The authors declare no competing financial interest.

■ ACKNOWLEDGMENTS

This work is financially supported by the National Natural Science Foundation of China (21275001 and 21422501 Y.X.; 21573002, Y.H.) and the Foundation for Innovation Team of Bioanalytical Chemistry.

■ REFERENCES

(1) (a) Henglein, A. *Chem. Rev.* **1989**, *89*, 1861−1873. (b) Daniel, M. C.; Astruc, D. *Chem. Rev.* **2004**, *104*, 293−346. (c) Saha, K.; Agasti, S. S.; Kim, C.; Li, X.; Rotello, V. M. *Chem. Rev.* **2012**, *112*, 2739−2779. (d) Kelly, K. L.; Coronado, E.; Zhao, L. L.; Schatz, G. C. *J. Phys. Chem. B* **2003**, *107*, 668−677. (e) Perrault, S. D.; Chan, W. C. W. *J. Am. Chem. Soc.* **2009**, *131*, 17042−17043.

(2) (a) Xie, X.; Xu, W.; Liu, X. *Acc. Chem. Res.* **2012**, *45*, 1511−1520. (b) Li, D.; Wieckowska, A.; Willner, I. *Angew. Chem., Int. Ed.* **2008**, *47*, 3927−3931.

(3) Liu, X.; Atwater, M.; Wang, J.; Huo, Q. *Colloids Surf., B* **2007**, *58*, 3−7.

(4) (a) Yang, X.; Yang, M.; Pang, B.; Vara, M.; Xia, Y. *Chem. Rev.* **2015**, *115*, 10410−10488. (b) Sapsford, K. E.; Algar, W. R.; Berti, L.; Gemmill, K. B.; Casey, B. J.; Oh, E.; Stewart, M. H.; Medintz, I. L. *Chem. Rev.* **2013**, *113*, 1904−2074. (c) Ray, P. C.; Fan, Z.; Crouch, R. A.; Sinha, S. S.; Pramanik, A. *Chem. Soc. Rev.* **2014**, *43*, 6370−6404.

(5) (a) Astruc, D.; Lu, F.; Aranzaes, J. R. *Angew. Chem., Int. Ed.* **2005**, *44*, 7852−7872. (b) Gorin, D. J.; Sherry, B. D.; Toste, F. D. *Chem. Rev.* **2008**, *108*, 3351−3378. (c) Lin, Y.; Ren, J.; Qu, X. *Adv. Mater.* **2014**, *26*, 4200−4217. (d) Luo, W.; Zhu, C.; Su, S.; Li, D.; He, Y.; Huang, Q.; Fan, C. *ACS Nano* **2010**, *4*, 7451−7458. (e) Yin, H.; Tang, H.; Wang, D.; Gao, Y.; Tang, Z. *ACS Nano* **2012**, *6*, 8288−8297.

(6) (a) Ghosh, S. K.; Pal, T. *Chem. Rev.* **2007**, *107*, 4797−4862. (b) Jain, P. K.; Lee, K. S.; El-Sayed, I. H.; El-Sayed, M. A. *J. Phys. Chem. B* **2006**, *110*, 7238−7248.

(7) Comotti, M.; Della Pina, C.; Matarrese, R.; Rossi, M. *Angew. Chem., Int. Ed.* **2004**, *43*, 5812−5815.

(8) (a) Bassanetti, I.; Comotti, A.; Sozzani, P.; Bracco, S.; Calestani, G.; Mezzadri, F.; Marchiò, L. *J. Am. Chem. Soc.* **2014**, *136*, 14883−14895. (b) Guo, D. S.; Liu, Y. *Chem. Soc. Rev.* **2012**, *41*, 5907−5921. (c) Yang, L.; Tan, X.; Wang, Z.; Zhang, X. *Chem. Rev.* **2015**, *115*, 7196−7239.

(9) (a) Dsouza, R. N.; Pischel, U.; Nau, W. M. *Chem. Rev.* **2011**, *111*, 7941−7980. (b) Chen, Y.; Liu, Y. *Adv. Mater.* **2015**, *27*, 5403−5409.

(10) (a) Descalzo, A. B.; Martínez-Máñez, R.; Sancenón, F.; Hoffmann, K.; Rurack, K. *Angew. Chem., Int. Ed.* **2006**, *45*, 5924−5948. (b) Qu, D. H.; Wang, Q. C.; Zhang, Q. W.; Ma, X.; Tian, H. *Chem. Rev.* **2015**, *115*, 7543−7588. (c) Yu, G.; Jie, K.; Huang, F. *Chem. Rev.* **2015**, *115*, 7240−7303. (d) Yang, Y. W.; Sun, Y. L.; Song, N. *Acc. Chem. Res.* **2014**, *47*, 1950−1960. (e) Liu, J.; Mendoza, S.; Román, E.; Lynn, M. J.; Xu, R.; Kaifer, A. E. *J. Am. Chem. Soc.* **1999**, *121*, 4304−4305. (f) Li, H.; Chen, D. X.; Sun, Y. L.; Zheng, Y. B.; Tan, L. L.; Weiss, P. S.; Yang, Y. W. *J. Am. Chem. Soc.* **2013**, *135*, 1570−1576. (g) Huang, T.; Meng, F.; Qi, L. *J. Phys. Chem. C* **2009**, *113*, 13636−13642. (h) Shi, Y.; Goodisman, J.; Dabrowiak, J. C. *Inorg. Chem.* **2013**, *52*, 9418−9426. (i) Celebioglu, A.; Uyar, T. *RSC Adv.* **2013**, *3*, 10197−10201.

(11) Persson, A. E.; Schoeman, B. J.; Sterte, J.; Otterstedt, J. E. *Zeolites* **1994**, *14*, 557−567.

(12) Turkevich, J.; Stevenson, P. C.; Hillier, J. *Discuss. Faraday Soc.* **1951**, *11*, 55−75.

(13) Zhu, H.; Du, M.; Zou, M.; Xu, C.; Li, N.; Fu, F. *J. Mater. Chem.* **2012**, *22*, 9301−9307.

(14) Bao, L.; Liu, C.; Zhang, Z. L.; Pang, D. W. *Adv. Mater.* **2015**, *27*, 1663−1667.

(15) Hu, S.; Trinchi, A.; Atkin, P.; Cole, I. *Angew. Chem., Int. Ed.* **2015**, *54*, 2970−2974.

(16) Xu, C.; Wang, J.; Wan, L.; Lin, J.; Wang, X. *J. Mater. Chem.* **2011**, *21*, 10463−10471.

(17) Schneider, H. J.; Hacket, F.; Rüdiger, V.; Ikeda, H. *Chem. Rev.* **1998**, *98*, 1755−1786.

(18) (a) Hurst, S. J.; Lytton-Jean, A. K. R.; Mirkin, C. A. *Anal. Chem.* **2006**, *78*, 8313−8318. (b) Alexander, C. M.; Dabrowiak, J. C.; Maye, M. M. *Bioconjugate Chem.* **2012**, *23*, 2061−2070.

(19) Smith, A. M.; Marbella, L. E.; Johnston, K. A.; Hartmann, M. J.; Crawford, S. E.; Kozycz, L. M.; Seferos, D. S.; Millstone, I. E. *Anal. Chem.* **2015**, *87*, 2771−2778.

(20) (a) Tao, Y.; Dai, J.; Kong, Y.; Sha, Y. *Anal. Chem.* **2014**, *86*, 2633−2639. (b) Khan, A. R.; Forgo, P.; Stine, K. J.; D'Souza, V. T. *Chem. Rev.* **1998**, *98*, 1977−1996.

(21) (a) Zhang, N.; Liu, Y.; Tong, L.; Xu, K.; Zhuo, L.; Tang, B. *Analyst* **2008**, *133*, 1176−1181. (b) Leung, F. C. M.; Au, V. K. M.; Song, H. O.; Yam, V. W. W. *Chem. - Eur. J.* **2015**, *21*, 16448−16454. (c) Mondal, A.; Jana, N. R. *Chem. Commun.* **2012**, *48*, 7316−7318.

(22) Sandberg, D. H.; Sjövall, J.; Sjövall, K.; Turner, D. A. *J. Lipid Res.* **1965**, *6*, 182−192.

(23) Guo, Y.; Guo, S.; Ren, J.; Zhai, Y.; Dong, S.; Wang, E. *ACS Nano* **2010**, *4*, 4001−4010.

(24) Olson, M. A.; Coskun, A.; Klajn, R.; Fang, L.; Dey, S. K.; Browne, K. P.; Grzybowski, B. A.; Stoddart, J. F. *Nano Lett.* **2009**, *9*, 3185−3190.

(25) (a) Cheng, W.; Campolongo, M. J.; Cha, J. J.; Tan, S. J.; Umbach, C. C.; Muller, D. A.; Luo, D. *Nat. Mater.* **2009**, *8*, 519−525. (b) Li, Y.; Liu, Z.; Yu, G.; Jiang, W.; Mao, C. *J. Am. Chem. Soc.* **2015**, *137*, 4320−4323. (c) Zhao, H.; Sen, S.; Udayabhaskararao, T.; Sawczyk, M.; Kučanda, K.; Manna, D.; Kundu, P. K.; Lee, J. W.; Král, P.; Klajn, R. *Nat. Nanotechnol.* **2016**, *11*, 82−88.

(26) (a) Lin, S.; Li, M.; Dujardin, E.; Girard, C.; Mann, S. *Adv. Mater.* **2005**, *17*, 2553−2559. (b) Han, X.; Li, Y.; Deng, Z. *Adv. Mater.* **2007**, *19*, 1518−1522.

(27) (a) Xia, Y.; Nguyen, T. D.; Yang, M.; Lee, B.; Santos, A.; Podsiadlo, P.; Tang, Z.; Glotzer, S. C.; Kotov, N. A. *Nat. Nanotechnol.* **2011**, *6*, 580−587. (b) Tang, Z.; Zhang, Z.; Wang, Y.; Glotzer, S. C.; Kotov, N. A. *Science* **2006**, *314*, 274−278.

(28) Murray, C. B.; Kagan, C. R.; Bawendi, M. G. *Science* **1995**, *270*, 1335−1338.

(29) Kotov, N. A. *Science* **2010**, *330*, 188−189.

(30) (a) Wei, H.; Wang, E. *Chem. Soc. Rev.* **2013**, *42*, 6060−6093. (b) Li, K.; Wang, K.; Qin, W.; Deng, S.; Li, D.; Shi, J.; Huang, Q.; Fan, C. *J. Am. Chem. Soc.* **2015**, *137*, 4292−4295.

(31) Rakitzis, E. T.; Papandreou, P. *Chem.-Biol. Interact.* **1998**, *113*, 205−216.

(32) Gao, L.; Zhuang, J.; Nie, L.; Zhang, J.; Zhang, Y.; Gu, N.; Wang, T.; Feng, J.; Yang, J.; Yang, D.; Perrett, S.; Yan, X. *Nat. Nanotechnol.* **2007**, *2*, 577−583.

(33) (a) Qu, K.; Shi, P.; Ren, J.; Qu, X. *Chem. - Eur. J.* **2014**, *20*, 7501−7506. (b) Zhao, M.; Deng, K.; He, L.; Liu, Y.; Li, G.; Zhao, H.; Tang, Z. *J. Am. Chem. Soc.* **2014**, *136*, 1738−1741.

(34) (a) Tian, N.; Zhou, Z. Y.; Sun, S. G.; Ding, Y.; Wang, Z. L. *Science* **2007**, *316*, 732−735. (b) Xia, Y.; Xiong, Y.; Lim, B.; Skrabalak, S. E. *Angew. Chem., Int. Ed.* **2009**, *48*, 60−103.
(35) Liu, Z.; Cai, R.; Mao, L.; Huang, H.; Ma, W. *Analyst* **1999**, *124*, 173−176.
(36) Henkelman, G.; Arnaldsson, A.; Jónsson, H. *Comput. Mater. Sci.* **2006**, *36*, 354−360.
(37) Comotti, M.; Della Pina, C.; Falletta, E.; Rossi, M. *Adv. Synth. Catal.* **2006**, *348*, 313−316.
(38) Ishibashi, K. I.; Fujishima, A.; Watanabe, T.; Hashimoto, K. *Electrochem. Commun.* **2000**, *2*, 207−210.
(39) Frey, A.; Meckelein, B.; Externest, D.; Schmidt, M. A. *J. Immunol. Methods* **2000**, *233*, 47−56.
(40) (a) Henglein, A. *J. Phys. Chem.* **1993**, *97*, 5457−5471. (b) Zhang, Z.; Berg, A.; Levanon, H.; Fessenden, R. W.; Meisel, D. *J. Am. Chem. Soc.* **2003**, *125*, 7959−7963.

DOI: 10.1021/jacs.6b07590
J. Am. Chem. Soc. 2016, 138, 16645−16654